Environmental Science & Technology

pubs.acs.org/est

Article

Significance of Non-DLVO Interactions on the Co-Transport of Functionalized Multiwalled Carbon Nanotubes and Soil Nanoparticles in Porous Media

Miaoyue Zhang, Scott A. Bradford, Erwin Klumpp, Jiri Šimůnek, Shizhong Wang, Quan Wan, Chao Jin,* and Rongliang Qiu

Cite This: https://doi.org/10.1021/acs.est.2c00681

Read Online

ABSTRACT: Derjaguin–Landau–Verwey–Overbeek (DLVO) theory is typically used to quantify surface interactions between engineered nanoparticles (ENPs), soil nanoparticles (SNPs), and/or porous media, which are used to assess environmental risk and fate of ENPs. This study investigates the co-transport behavior of functionalized multiwalled carbon nanotubes (MWCNTs) with positively (goethite nanoparticles, GNPs) and negatively (bentonite nanoparticles, BNPs) charged SNPs in quartz sand (QS). The presence of BNPs increased the transport of MWCNTs, but GNPs inhibited the transport of MWCNTs. In addition, we, for the first time, observed that the transport of negatively (BNPs) and positively (GNPs) charged SNPs was facilitated by the presence of MWCNTs. Traditional mechanisms associated with competitive blocking, heteroaggregation, and classic DLVO calculations cannot explain such phenomena. Direct examination using batch experiments and Fourier transform infrared (FTIR) spectroscopy, asymmetric flow field flow fractionation (AF4) coupled to UV and inductively coupled plasma mass spectrometry (AF4-UV-ICP-MS), and molecular dynamics (MD) simulations demonstrated that MWCNTs-BNPs or MWCNT-GNPs complexes or aggregates can be formed during co-transport. Non-DLVO interactions (e.g., H-bonding and Lewis acid–base interaction) helped to explain observed MWCNT deposition, associations between MWCNTs and both SNPs (positively or negatively), and co-transport. This research sheds novel insight into the transport of MWCNTs and SNPs in porous media and suggests that (i) mutual effects between colloids (e.g., heteroaggregation, co-transport, and competitive blocking) need to be considered in natural soil; and (ii) non-DLVO interactions should be comprehensively considered when evaluating the environmental risk and fate of ENPs.

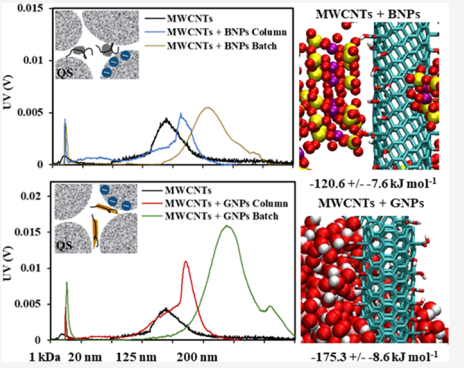

KEYWORDS: *multiwalled carbon nanotubes, soil nanoparticles, colloid-facilitated transport, molecular dynamics simulation, asymmetric flow field flow fractionation*

INTRODUCTION

Carbon nanotubes (CNTs) are allotropes of carbon with a cylindrical-shaped nanostructure[1] that have unique electric, chemical, and physical properties. CNTs have been employed in numerous commercial applications and as adsorbents for environmental remediation and water treatment,[2−6] which will eventually result in their release into the subsurface.[7] Current studies have investigated the transport behavior of CNTs in porous media under various physical and chemical conditions, including ionic strength (IS), water content, porous medium grain size, input concentration of CNTs, surfactants, and organic matter.[8−13] However, information on the co-transport of CNTs and soil colloids or soil nanoparticles (SNPs), as well as interactions of CNTs with soil colloids or SNPs is still limited.

SNPs (e.g., clay minerals and iron oxides), which are abundant in the Earth's critical zone[14,15] and the smaller size fractions (<100 nm in at least one dimension) in soil colloids, can serve as carriers for contaminants and result in colloid-facilitated contaminant transport.[16] Colloid-facilitated contaminant transport has been demonstrated to be one of the critical pathways for the long-distance transport of contaminants in soil and groundwater. Such processes are mainly governed by interactions between colloids and dissolved contaminants like heavy metals, rare earth elements, and organic pollutants. A few recent studies have demonstrated that soil colloids also facilitate the co-transport of other colloids (e.g., engineered nanoparticles (ENPs) and biocolloids), such as titanium dioxide nanoparticles with clay particles,[17] bacteria with

Received: January 28, 2022
Revised: June 8, 2022
Accepted: June 8, 2022

hematite,[18] viruses with clay colloids,[19−21] and plastic particles with iron oxides.[22,23] Clay minerals and iron oxides are common SNPs that ENPs can encounter in soil. However, the co-transport of ENPs and SNPs has received limited attention. Mechanisms explaining the unique deposition behavior of CNT in the presence of SNP in porous media are still not available in the literature.

The unique chemical and physical properties are commonly introduced on the surface of ENPs when they are manufactured (e.g., material doping, modification) by regulating surface moieties or functional groups to achieve designed functionality (e.g., superhydrophobic/hydrophilic, antifouling, self-cleaning, etc).[24,25] In contrast, SNPs are much more complex than ENPs because of the presence of both roughness and charge heterogeneity. In addition to van der Waals (VDW) and electrical double-layer (EDL) interactions, the formation of SNP−ENP associations may also be impacted by H-bonding and Lewis acid−base interactions.[26−28] However, only a few studies have attempted to differentiate the relative contribution of these interactions on aggregation and retention processes in porous media.

Most previous studies[17,29] attempted to interpret the deposition of ENPs in porous media using coulombic interactions (e.g., negative vs positive charge interactions), whereas competitive blocking was regarded as the main mechanism for enhanced transport of colloids.[22,30,31] Additionally, investigations on the effect of soil colloids (e.g., micro-sized clay minerals or iron oxides) on the transport and retention of ENPs in porous media were frequently conducted at high input concentrations of ENPs and low concentrations of soil colloids.[22,30] Such studies ignored the fact that the total concentration of colloids/SNPs in soil is significantly higher than the discharged concentration of ENPs.

DLVO theory assumes that colloid aggregation and retention are mainly controlled by interactions that arise from VDW and EDL forces. The transport behavior of colloids can sometimes be reasonably described by quantifying these interactions.[22,32,33] For example, heteroaggregation between carbon nanoparticles and mineral colloids resulted in sedimentation of carbon nanoparticles due to reduced electrostatic repulsion.[26,34] However, some recent studies indicated that ENPs (e.g., CNTs) could exhibit different transport behavior from classic colloid filtration theory (CFT) and DLVO theory.[27,35] For example, Katzourakis and Chrysikopoulos indicated that aggregation could contribute to the attachment of ENPs in porous media.[33] Liu et al.[27] and Yang et al.[28] indicated that chemical bonds were formed between carbon dots and minerals, as well as biochar and bentonite, in batch and aggregation experiments, respectively. Soil colloids and ENPs were also found to be strongly associated during transport experiments, even under variable flow conditions.[36] It was hypothesized that attachment/detachment and aggregation of ENPs might be influenced by other surface interactions such as H-bonding, Lewis acid−base interactions/reactions, ligand exchange, and other chemical reactions. DLVO interactions are weakly or nondirectional, whereas non-DLVO interactions are commonly orientational-dependent and preferentially associated with specific surface functional groups.[37] Co-transport has usually been attributed to the strong affinity between soil colloids and ENPs, but has neglected the role of non-DLVO interactions (e.g., H-bonding, Lewis acid−base, and ligand exchange). Interaction, association, and co-transport of ENPs and soil colloids/SNPs are complex, and there are still many questions. For example, if heteroaggregation occurs during the co-transport of ENPs and soil colloids/SNPs, will the transport of ENPs be facilitated or inhibited? Can attached ENPs contribute to the retention of soil colloids/SNPs in porous media?

The objective of this study is to investigate mechanisms that govern the co-transport and retention of functionalized MWCNTs (1 mg L^{-1}) and SNPs. Breakthrough curves (BTCs) and retention profiles (RPs) for both MWCNTs and negatively charged bentonite nanoparticles (BNPs, at 0−10 mg L^{-1}) or positively charged goethite nanoparticles (GNPs, at 0−4 mg L^{-1}) were determined in column tests. Mechanisms that contribute to the co-transport and competitive blocking behaviors were quantified numerically using the HYDRUS-1D computer code. Direct experimental evidence was obtained to identify the association between MWCNTs and SNPs using batch experiments, transmission electron microscopy (TEM), asymmetric flow field flow fractionation (AF4) combined with UV and inductively coupled plasma mass spectrometry (AF4-UV-ICP-MS), as well as Fourier transform infrared (FTIR) spectroscopy. Classic DLVO calculations and molecular dynamics (MD) simulations were conducted and compared to elucidate further the role of non-DLVO interactions between SNPs and MWCNTs on their deposition in porous media. Such analysis provides essential knowledge and a research roadmap to evaluate the environmental risks of MWCNTs and other emerging ENPs in natural environments.

MATERIALS AND METHODS

Carbon Nanotubes, Bentonite Nanoparticles, and Goethite Nanoparticles. Radioactively (^{14}C) labeled MWCNTs (Bayer Technology Services GmbH, Leverkusen, Germany) with a median diameter of 10−15 nm and a median length of 200−1000 nm[38] were used in this study. More information on the synthesis, functionalization, and characterization of these MWCNTs is available in the literature.[13] The functionalization of MWCNTs resulted in the addition of oxygen-containing groups (e.g., carboxylic groups) to their surface. Bentonite and goethite colloids were purchased from Sigma-Aldrich Chemie GmbH (Munich, Germany). More information on the preparation of BNPs and GNPs is summarized in Section S1. Briefly, the prepared BNPs had a diameter of 5−200 nm (Figure S1a), and GNPs had a diameter of 5−120 nm and a length of 60−800 nm (Figure S1b). The MWCNTs (0 and 1 mg L^{-1}) and BNPs (0, 4, and 10 mg L^{-1}) or GNPs (0, 2, and 4 mg L^{-1}) suspensions were prepared in IS = 1 mM KCl (pH = 5.4). The suspension of MWCNTs and/or SNPs (BNPs or GNPs) was ultrasonicated for 15 min at 65 W and again for 10 min before characterization and column experiments discussed below. The concentration of ^{14}C-labeled MWCNTs was determined using a PerkinElmer (Rodgau) liquid scintillation counter (LSC). Radioactively (^{14}C)-labeled MWCNTs are stable, and the attenuation of the radio signal during the column experiments (<1 h) could be neglected. The concentrations of BNPs and GNPs were determined from the measurement of Al and Fe concentrations, respectively, by inductively coupled plasma mass spectrometry (ICP- MS, Agilent 7500) after digestion and dilution.

The hydrodynamic radius of the MWCNTs suspensions in IS = 1 mM KCl at different concentrations of BNPs (0, 4, and 10 mg L^{-1}) or GNPs (0, 2, and 4 mg L^{-1}) was measured using a Zetasizer Nano (Malvern Instruments GmbH, 71083

https://doi.org/10.1021/acs.est.2c00681
Environ. Sci. Technol. XXXX, XXX, XXX−XXX

Table 1. Experimental Conditions and Mass Recoveries from Effluent for All Column Experiments; D_{50} = 240 μm[a]

$C_{o(M)}$ [mg L^{-1}]	$C_{o(b)}$ [mg L^{-1}]	$C_{o(g)}$ [mg L^{-1}]	q [cm min^{-1}]	IS [mM]	Por.	M_{e_M} [%]	M_{s_M} [%]	M_{t_M} [%]	M_{e_S} [%]	M_{s_S} [%]	M_{t_S} [%]
1	0	0	0.72	1 K^+	0.45	15.7	76.2	91.9	NA	NA	NA
0	4	0	0.71	1 K^+	0.45	NA	NA	NA	24.9	70.2	95.1
0	0	4	0.71	1 K^+	0.44	NA	NA	NA	8.8	87.9	96.7
1	4	0	0.71	1 K^+	0.46	18.5	75.5	94.0	31.7	60.3	92.0
1	10	0	0.71	1 K^+	0.43	23.1	70.6	93.7	40.5	55.0	95.5
1	0	2	0.71	1 K^+	0.45	1.2	96.3	97.5	20.2	75.7	95.9
1	0	4	0.72	1 K^+	0.46	1.1	99.9	101.0	21.4	74.3	95.7

[a]NA denotes not applicable. *Por.* is the porosity of the column. $C_{o(M)}$, $C_{o(b)}$, and $C_{o(g)}$ are the input concentrations of MWCNTs, BNPs, and GNPs, respectively. q is the Darcy velocity. M_{e_M}, M_{s_M}, and M_{t_M} are the effluent percentage, retained percentage, and total percentage of MWCNTs recovered from the column experiment, respectively. M_{e_S}, M_{s_S}, and M_{t_S} are the effluent, solid, and total percentage of SNPs (BNPs or GNPs) recovered in the column experiments, respectively.

Herrenberg, Germany) immediately after suspension preparation and after 1 h. This information was used to determine the stability of these suspensions.[39,40] In particular, the hydrodynamic radii of all suspensions were within the same range at 0 and 1 h, which indicates that these suspensions were stable during this time interval. The release of Al and Fe ions was also determined to be negligible after the preparation of BNPs and GNPs suspensions at 1 h.

Interaction Energy Calculations. The approach of Bradford and Torkzaban[41] was used to calculate the total interaction energy (Φ) between a planar quartz surface and a spherical colloid with similar properties to MWCNTs in the presence of various concentrations of BNPs or GNPs in KCl solution with an IS = 1 mM. The total interaction energies between MWCNTs, MWCNTs and BNPs, and MWCNTs and GNPs were also performed to help explain the aggregation behavior between them. Other non-DLVO interactions (e.g., steric forces, hydration effects, and Lewis acid−base forces) were not considered. Details pertaining to these calculations are given in Section S2.

Batch Experiments. Batch experiments were conducted using SNPs (BNPs or GNPs) and MWCNTs in accordance with the Organization for Economic Cooperation and Development (OECD)—guideline 106.[42] Section S3 provides details about the batch experiments. In brief, batch experiments were carried out under quasi-equilibrium conditions[43,44] in 1 mM KCl solution. FTIR spectroscopy (Nicolet 6700, Thermo Fisher) was conducted after batch experiments to characterize the associations between SNPs (BNPs or GNPs) and MWCNTs.

Co-Transport Experiments. A stainless-steel column with 3 cm inner diameter and 12 cm length was uniformly wet packed with purified quartz sand (QS, median grain size of 240 μm).[11,43] Approximately 30 pore volumes (PVs) of background electrolyte solution (1 mM KCl) were injected at a constant Darcy velocity of 0.71−0.72 cm min^{-1} to equilibrate the column before initiating an experiment.

A non-reactive (conservative) tracer experiment was conducted to characterize the column's hydraulic conditions. Concentrations of bromide in the effluent were determined using a high-performance liquid chromatograph (STH 585, Dionex, Sunnyvale, CA) equipped with a UV detector (UV2075, Jasco, Essex, U.K.). Transport experiments using MWCNTs (0 and 1 mg L^{-1}) and SNPs (0, 4, and 10 mg L^{-1} BNPs or 0, 2, and 4 mg L^{-1} GNPs) in 1 mM KCl solution were conducted in a similar manner as the conservative tracer. Single-particle ICP-MS has been demonstrated to quantify the environmental concentrations of metal nanoparticles,[45−47] but this methodology cannot determine concentrations of carbon-based nanoparticles. The input concentrations of MWCNTs and SNPs were selected based on the results of preliminary aggregation experiments with MWCNTs and SNPs (data not shown). An input concentration of 1 mg L^{-1} of MWCNTs was employed to obtain high accuracy in transport studies. The RPs of MWCNTs and SNPs (BNPs or GNPs) in column studies were determined following the recovery of BTCs and excavation of QS in 1 cm increments. The concentrations of MWCNTs and BNPs or GNPs in the effluent and sand were determined using the LSC and ICP-MS, respectively.

All BTCs are plotted herein as normalized effluent concentrations (C/C_o; where C_o is the influent suspension concentration) vs pore volumes. All RPs are given herein as normalized solid-phase concentration (S/C_o) as a function of distance from the column inlet. Experiments were replicated and exhibited good reproducibility. A summary of the experimental conditions, including Darcy velocity and mass balance information, is provided in Table 1. The total mass balance for MWCNTs (M_{t_M}) and SNPs (M_{t_S}) in the column experiments was very good (>91%, Table 1).

Numerical Modeling. A modified version of the HYDRUS-1D computer code[48] was employed to simulate both the transport and retention of MWCNTs and SNPs (BNPs or GNPs) in QS. The mass balance equations in the aqueous and solid phases for MWCNTs are given as

$$\frac{\partial C_M}{\partial t} = \frac{\partial}{\partial z}\left(D\frac{\partial C_M}{\partial z}\right) - \frac{\partial(vC_M)}{\partial z} - \psi_M k_{Ma} C_M + \frac{\rho_b}{\theta} k_{Md} S_M \quad (1)$$

$$\rho\frac{\partial S_M}{\partial t} = \theta\psi_M k_{Ma} C_M - \rho_b \rho k_{Md} S_M \quad (2)$$

where D is the dispersion coefficient, C_M is the aqueous phase concentration, S_M is the solid-phase concentration, v is the pore water velocity, k_{Ma} is the retention rate coefficient, k_{Md} is the detachment rate coefficient, z is the vertical distance, t is the time, ρ_b is the bulk density, and θ is the porosity. The parameter ψ_M is a dimensionless function to account for time- and depth-dependent retention and is given in this work as

$$\psi_M = \left(1 - \frac{S_M + \Gamma_M S_S}{S_M^{max}}\right)\left(\frac{d_{50} + z}{d_{50}}\right)^{-\beta} \quad (3)$$

where S_M^{max} is the maximum solid-phase concentration, d_{50} is the median grain size, Γ_M is the area conversion factor between SNPs (BNPs or GNPs) and MWCNTs, and β is an empirical parameter that controls the shape of the retention profile. The

https://doi.org/10.1021/acs.est.2c00681
Environ. Sci. Technol. XXXX, XXX, XXX−XXX

Table 2. Fitted Model Parameters[a]

model	AIC_M	AIC_S	AIC_{M+C}	S_M^{max}/C_o [cm^3 g^{-1}]	Γ_M	k_{Ma} [min^{-1}]	S_S^{max}/C_o [cm^3 g^{-1}]	Γ_S	k_{Sa} [min^{-1}]	R_{Meff}^2	R_{Ms}^2	R_{Seff}^2	R_{Ss}^2
				$C_{o\ (MWCNTs)}$ = 1 mg L^{-1}, $C_{o\ (BNPs/GNPs)}$ = 0 mg L^{-1}, 1 mM KCl									
M1	241.4	NF	1.689	NF	16.45	NF	NF	NF	0.987	0.908	NF	NF	
				$C_{o\ (MWCNTs)}$ = 0 mg L^{-1}, $C_{o\ (BNPs)}$ = 4 mg L^{-1}, 1 mM KCl									
M1	NF	−89.9	NF	NF	NF	2.264	NF	10.72	NF	NF	0.989	0.981	
				$C_{o\ (MWCNTs)}$ = 0 mg L^{-1}, $C_{o\ (GNPs)}$ = 4 mg L^{-1}, 1 mM KCl									
M1	NF	291.2	NF	NF	NF	2.881	NF	22.91	NF	NF	0.620	0.993	
				$C_{o\ (MWCNTs)}$ = 1 mg L^{-1}, $C_{o\ (BNPs)}$ = 4 mg L^{-1}, 1 mM KCl									
M1	−329.1		1.639	NF	14.29	2.247	NF	9.88	0.993	0.971	0.986	0.980	
M2	−326.9		1.639	2.35×10^{-3}	14.29	2.247	7.57×10^{-4}	9.88	0.993	0.971	0.986	0.980	
				$C_{o\ (MWCNTs)}$ = 1 mg L^{-1}, $C_{o\ (BNPs)}$ = 10 mg L^{-1}, 1 mM KCl									
M1	−155.2		1.270	NF	14.12	1.724	NF	9.65	0.984	0.995	0.940	0.971	
M2	−157.7		1.270	1.10×10^{-1}	14.12	1.724	1.97×10^{-2}	9.65	0.984	0.995	0.941	0.974	
				$C_{o\ (MWCNTs)}$ = 1 mg L^{-1}, $C_{o\ (GNPs)}$ = 2 mg L^{-1}, 1 mM KCl									
M1	−279.1		1.734	NF	46.66	2.492	NF	14.32	0.94	0.980	0.654	0.996	
M2	−285.0		1.734	3.25×10^{-3}	46.66	2.492	1.61×10^{-1}	14.32	0.942	0.977	0.680	0.996	
				$C_{o\ (MWCNTs)}$ = 1 mg L^{-1}, $C_{o\ (GNPs)}$ = 4 mg L^{-1}, 1 mM KCl									
M1	−235.8		1.845	NF	47.11	2.402	NF	14.08	0.974	0.941	0.899	0.990	
M2	−220.0		1.845	1.52×10^{-3}	47.11	2.402	6.90×10^{-2}	14.08	0.973	0.941	0.899	0.990	

[a] S_M^{max}/C_o and k_{Ma} are the normalized maximum solid-phase concentration and the first-order retention rate coefficient of MWCNTs, respectively; S_S^{max}/C_o and k_{Sa} are the normalized maximum solid-phase concentration and the first-order retention rate coefficient of SNPs (BNPs or GNPs), respectively; NF denotes not fitted; R_{Meff}^2, R_{Ms}^2, R_{Seff}^2, and R_{Ss}^2 are the correlation of observed and fitted data for MWCNTs in the effluent, MWCNTs in the solid phase, SNPs (BNPs or GNPs) in the effluent, and SNPs (BNPs or GNPs) in the solid phase, respectively. AIC_M and AIC_S are the Akaike information criterion for MWCNTSs and SNPs (BNPs or GNPs) in the M1 model, respectively. AIC_{M+S} is the Akaike information criterion for MWCNTSs and SNPs (BNPs or GNPs) in co-transport. Γ_M is the area conversion factor between SNPs (BNPs or GNPs) and MWCNTs. Γ_S is the area conversion factor between MWCNT and SNPs (BNPs or GNPs). The fitted parameters of dispersion coefficient, k_{Md}, and k_{Sd} are in Table S2.

subscripts *M* and *S* on parameters indicate that they are associated with MWCNTs and SNPs, respectively. Similar equations are employed for SNPs when the subscript M is replaced by S in eqs 1−3. Aggregation, particle size distributions, and co-transport were assumed to play relatively minor roles under the experimental conditions and were not accounted for in the simulations, but the co-authors have developed other models for this purpose.[49,50]

M1 and M2 models considering no and limited competitive blocking, respectively, were used to simulate the co-transport of MWCNTs and SNPs in the column experiments. Competitive blocking between MWCNTs and SNPs on the QS was accounted for in the M2 model using a Langmuirian blocking approach that was modified to include area conversion factors between MWCNTs and SNPs, Γ_M and Γ_S, respectively. The single-species transport of MWCNTs and SNPs (BNPs or GNPs) were described by setting Γ_M and Γ_S to zero, respectively. The transport and retention parameters for MWCNTs and SNPs (BNPs or GNPs) data sets were independently determined when using the M1 approach. The M2 approach allows for competitive blocking by fixing the retention and release parameters to those determined from the M1 model, and then simultaneously optimizing values of Γ_M and Γ_S to both MWCNTs and SNPs (BNPs or GNPs) data sets. Parameters for model fitting are given in Tables 2 and S2, along with the Pearson correlation coefficient (R^2) and Akaike information criterion (AIC),[51] representing the goodness of fit. More details about simulation equations are provided in Section S4.

Online-Coupled AF4-UV-ICP-MS Analyses. The effluent samples in co-transport experiments using MWCNTs (1 mg L^{-1}) and SNPs (4 mg L^{-1} BNPs or GNPs) in 1 mM KCl were measured using transmission electron microscopy (TEM, Hitachi SU8010, Japan), and AF4 (Postnova, Landsberg, Germany) combined online with UV and inductively coupled plasma mass spectrometer (AF4-UV-ICP-MS). The solid samples after batch experiments were diluted by 1 mM KCl and sonicated, and then also measured by AF4-UV-ICP-MS. The association between MWCNTs and SNPs, the hydrodynamic particle sizes, the intensities of UV, and the concentrations of iron (Fe) and aluminum (Al) (proxies for GNP and BNP, respectively) were determined using this approach. A 1 kDa polyethersulfone (PES) membrane and a carrier solution of 25 μM NaCl were used during the measurement. To separate small particles, 1 mL from the effluent sample was injected with a focus time of 20 min at a cross-flow of 3 mL min^{-1}. The particles were then separated by a linear cross-flow decrease for 40 min after focusing. The largest particles were flushed last at a constant cross-flow of 0 mL min^{-1} for 20 min. The particle size distribution of the AF4 separation was verified using latex standards with sizes of 20, 125, and 200 nm (from Postnova Analytics).[52,53] Figure S2 shows blanks for single BNPs and GNPs suspensions in AF4-UV-ICP-MS measurement (4 mg L^{-1}, 1 mM KCl).

Molecular Dynamics Simulations. The all-atom MD simulations were based on a Charmm36 force field[54,55] and were carried out using the Gromacs-4.6.7 software package.[56] The time step was 2 fs, and the total run time was 10 ns NPT for the equilibrium MD simulation. The relaxed system was employed as a starting configuration. Energy minimization was carried out prior to system relaxation with a composite protocol of steepest descent using termination gradients of 100 kJ (mol·nm)$^{-1}$. The Nose−Hoover thermostat[57] was used to maintain the equilibrium temperature at 298 K and 1 bar with

https://doi.org/10.1021/acs.est.2c00681
Environ. Sci. Technol. XXXX, XXX, XXX−XXX

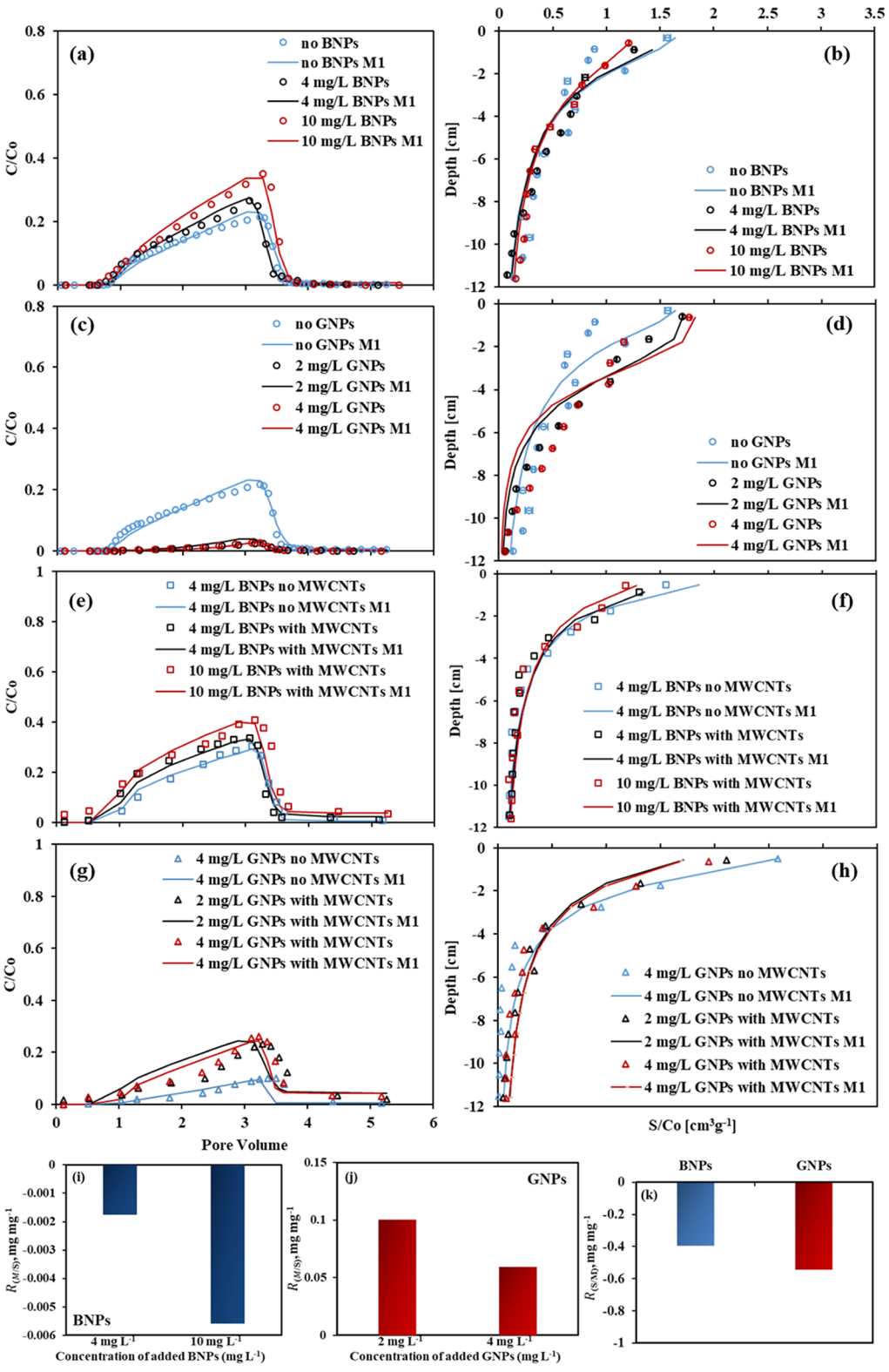

Figure 1. Observed and fitted (M1 model) BTCs (a, c, e, g) and RPs (b, d, f, h) of MWCNTs and SNPs (BNPs or GNPs) with or without additional SNPs in QS. The observed and fitted (M2 model) BTCs and RPs of MWCNTs and SNPs are shown in Figure S3. (a) BTCs of MWCNTs with adding 0, 4, and 10 mg L^{-1} of BNPs; (b) RPs of MWCNTs with adding 0, 4, and 10 mg L^{-1} of BNPs; (c) BTCs of MWCNTs with adding 0, 2, and 4 mg L^{-1} of GNPs. (d) RPs of MWCNTs with adding 0, 2, and 4 mg L^{-1} of GNPs. (e) BTCs of BNPs with and without MWCNTs at 4 and 10 mg L^{-1} of BNPs; (f) RPs of BNPs with and without MWCNTs at 4 and 10 mg L^{-1} of BNPs; (g) BTCs of GNPs with and without MWCNTs at 2 and 4 mg L^{-1} of BNPs. (h) RPs of GNPs with and without MWCNTs at 2 and 4 mg L^{-1} of BNPs; (i, j) mass ratio of retained MWCNTs and retained BNPs and GNPs in co-transport experiments, respectively; (k) mass ratio of retained SNPs (BNPs or GNPs) and retained MWCNTs in co-transport experiments. The input concentration of MWCNTs was 1 mg L^{-1}. The ionic strength was 1 mM KCl. The Darcy velocity is 0.71−0.72 cm min^{-1}.

https://doi.org/10.1021/acs.est.2c00681
Environ. Sci. Technol. XXXX, XXX, XXX−XXX

periodic boundary conditions imposed on all three dimensions. The particle mesh-Ewald method[58,59] was used to compute long-range electrostatics with a relative tolerance of 1×10^{-6}. A cutoff distance of 1.2 nm was applied to real-space Ewald and van der Waals interactions. The LINCS algorithm[60] was applied to constrain bond lengths of hydrogen atoms. A leap-frog algorithm was used with a time step of 2 fs. The mean distance between the centroids of MWCNTs, as well as the binding energies and binding mechanism of MWCNTs, in the presence of SNPs (BNPs or GNPs) were determined.

RESULTS AND DISCUSSION

Contribution of BNPs and GNPs to MWCNT Transport. Observed and simulated (M1 and M2 models) BTCs and RPs of MWCNTs with and without the negatively charged BNPs in the QS packed column are presented in Figure 1a,b. MWCNTs exhibited similar breakthrough behavior in the presence and absence of BNPs (Figure 1a); e.g., a breakthrough occurred after ∼1 PV, and then normalized effluent concentration gradually increased with continuous injection of MWCNTs. Co-injected of BNPs with MWCNTs resulted in higher effluent concentrations of MWCNTs. The recovered mass percentage of MWCNTs in the effluent increased from 15.7 to 23.1% when the C_o of BNPs increased from 0 to 10 mg L^{-1} (Figure 1a and Table 1), respectively. The effluent concentrations of MWCNTs rapidly decreased to low tailing values ($C/C_o < 0.02$) after the eluting suspension was switched to a colloid-free solution. The asymmetric shape of the BTCs was reasonably described by the implemented M1 model with Langmuirian blocking ($R^2 > 0.94$ in Table 2). The corresponding RPs for MWCNTs (Figure 1b), which exhibited hyper-exponential shapes along the direction of flow injection, were effectively simulated ($R^2 > 0.97$ in Table 2) using the M1 model associated with a depth-dependent retention function ($\beta = 0.765$). It should be noted that fitted values of k_{Ma} and S_M^{max}/C_o all decreased with increasing BNP concentration (Table 1). Such results suggested that increasing concentrations of BNPs could facilitate MWCNT transport.

The observed and simulated BTCs and RPs of MWCNTs with and without positively charged GNPs (in the packed column) are presented in Figure 1c,d. The transport of MWCNTs was diminished in the presence of GNPs (2 and 4 mg L^{-1}) compared to ones without GNPs. In particular, the mass percentage of MWCNTs that was recovered in the effluent (M_{e_M}, Figure 1c and Table 1) decreased from 15.7 to 1.1% when the input concentration of GNPs increased from 0 to 4 mg L^{-1}, respectively. A higher GNP concentration was also associated with an increase in the solid-phase mass percentage (e.g., 76.2−99.9%) for MWCNTs (Table 1 and Figure 1d). The BTCs for MWCNTs in the presence of GNPs (Figure 1c) ($R^2 > 0.94$ in Table 2) and the RPs for MWCNTs (Figure 1d) and GNPs ($R^2 > 0.91$ in Table 2) were also well described using the M1 model. Note that fitted values of k_{Ma} were very large in the presence of GNPs (Table 2), and this delayed the breakthrough of MWCNT until blocking decreased the number of available retention sites. The values of k_{Ma} and S_M^{max}/C_o for MWCNTs increased with the GNP concentration (Table 2). These results collectively suggested that although the retention of positively charged GNPs on the negatively charged QS surface was commonly regarded as an electrostatically favorable process, the observed blocking behavior for GNPs indicated that there was only a limited fraction of retention sites available for GNPs on the QS. These "favorable sites" on the surface of QS were rapidly filled under the selected conditions. Increasing the concentration of GNPs produced more inhibition of the transport of MWCNTs in packed QS.

Enhanced Transport of BNPs and GNPs. The presence of MWCNTs enhanced the transport of both the BNPs and GNPs in the packed column. The mass percentage recovered in the effluent for BNPs (M_{e_S}, Figure 1e and Table 1) increased from 24.9 to 31.7% when the MWCNTs C_o increased from 0 to 1 mg L^{-1}. This was associated with a decrease in the solid-phase mass percentage of BNPs (M_{s_S}, Figure 1f and Table 1). Similarly, the breakthrough of GNPs increased from 8.8 to 21.4% (Figure 1g and Table 1), whereas the corresponding GNPs solid-phase mass recovery (M_{s_S}, Figure 1h and Table 1) decreased when the concentration of MWCNTs increased. All of the BTCs for BNPs (Figure 1e) and most of the BTCs for GNPs (Figure 1g) were well described using the M1 model ($R^2 > 0.94$ and 0.62 for BNPs and GNPs, respectively, in Table 2). Fitted values of k_{Sa} and S_S^{max}/C_o for BNPs decreased with increasing BNPs concentration. Fitted values of k_{Sa} and S_S^{max}/C_o for GNPs were high, but only slightly decreased with increasing GNPs concentration. Interestingly, fitted values of k_{Sa} and S_S^{max}/C_o were sometimes larger for negatively charged BNPs than that for positively charged GNPs (Table 2). This observation indicated that electrostatically favorable conditions were not the only factors contributing to the limited goethite retention. Zhang et al.[43] previously found that not all of the surface area of goethite-coated sand contributed to MWCNT retention due to nanoscale roughness that creates shallow primary minimum interactions. The observation of rapid blocking of goethite colloids on QS was consistent with this finding. The values of k_{Sa} and S_S^{max}/C_o for BNPs and GNPs were lower in the presence than in the absence of MWCNTs (Table 2). The corresponding RPs for both MWCNTs and SNPs exhibited hyper-exponential shapes (Figure 1). This was accounted for in the M1 model by using a depth-dependent retention function with $\beta = 0.765$. Note that previous studies with MWCNTs have attributed this depth-dependent retention behavior to straining.[61−63]

The net mass of MWCNTs that was retained due to SNPs ($R_{M/S}$) and the net mass of SNPs that was retained due to MWCNTs ($R_{S/M}$) were quantified to evaluate mutual contributions. Values of $R_{M/S}$ and $R_{S/M}$ were calculated using eqs 4 and 5, respectively, as

$$R_{M/S} = \frac{\Delta R_M}{R_S} \tag{4}$$

$$R_{S/M} = \frac{\Delta R_S}{R_M} \tag{5}$$

where ΔR_M is the difference in retained mass of MWCNTs in the presence and absence of SNPs, ΔR_S is the difference in retained mass of SNPs in the presence and absence of MWCNTs, and R_S and R_M are the injected masses of SNPs and MWCNTs, respectively. Note that ΔR_M and ΔR_S have subtracted the corresponding single-species results to reflect the retained mass of MWCNTs due to SNPs on co-transport. The values of $R_{M/S}$ and $R_{S/M}$, therefore, reflect the net mass of MWCNTs and SNPs that were retained due to attached SNPs and MWCNTs, respectively.

https://doi.org/10.1021/acs.est.2c00681
Environ. Sci. Technol. XXXX, XXX, XXX−XXX

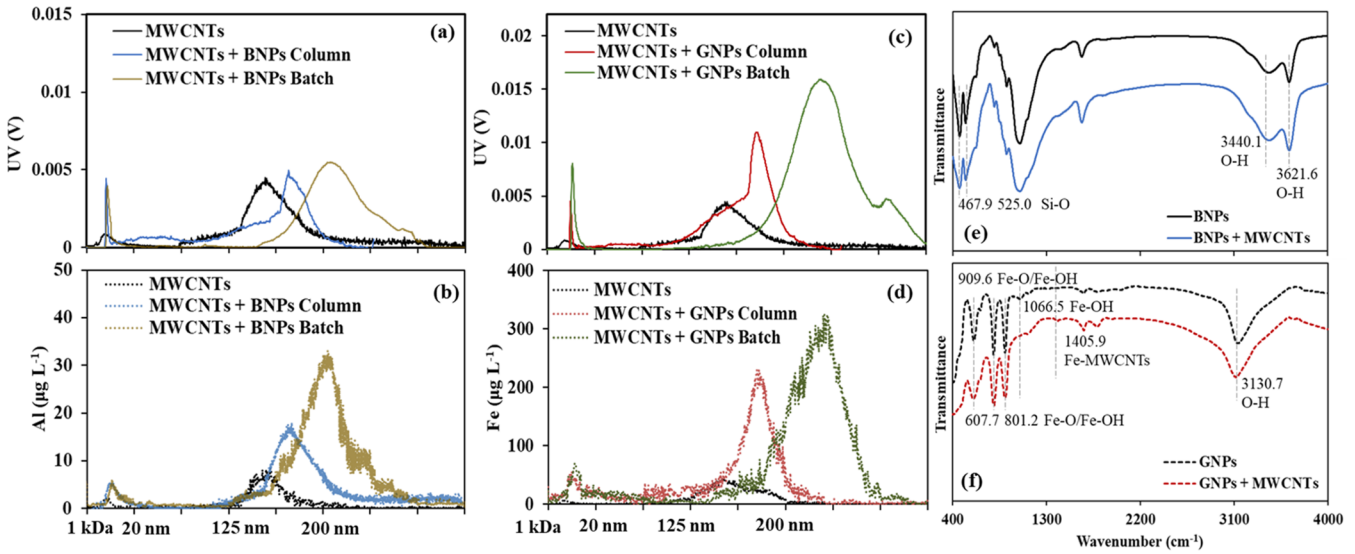

Figure 2. AF4 fractograms (a–d) of MWCNTs associated with BNPs or GNPs in the effluent during the co-transport experiments (1 mg L^{-1} MWCNTs with 4 mg L^{-1} BNPs or GNPs, 1 mM KCl) and FTIR spectra of BNPs (e) and GNPs (f) before and after attachment with MWCNT at 1 mM KCl. (a, c) Intensities of UV (V) and (b, d) concentrations of Al (μg L^{-1}) and Fe (μg L^{-1}), respectively, for MWCNTs + BNPs and MWCNTs + GNPs. The concentration of single MWCNT suspension for AF4-UV-ICP-MS measurement was 1 mg L^{-1} (1 mM KCl).

Calculated values of $R_{M/S}$ (mg mg^{-1}) are shown in Figure 1i,j as a function of BNPs and GNPs, respectively, whereas $R_{S/M}$ (mg mg^{-1}) is given in Figure 1k as a function of MWCNTs. It was found that values of $R_{M/S}$ were -1.8×10^{-3} and -5.7×10^{-3} mg mg^{-1} when the concentration of BNP was 4 and 10 mg L^{-1} (Figure 1i) but changed to 0.1 and 5.9E-02 mg mg^{-1} when the concentration of GNP was 2 and 4 mg L^{-1} (Figure 1j), respectively. Negative values of $R_{M/S}$ indicate that BNPs attached on the MWCNTs decrease the MWCNTs retention, whereas positive values show an enhancement in MWCNTs retention due to GNPs attachment. Additionally, retention was hindered for both BNPs and GNPs due to the attachment of MWCNTs. Note that the $R_{M/S}$ values for MWCNTs increased with increasing BNPs concentration (Figure 1i), while the $R_{M/S}$ values of MWCNTs decreased with increasing GNPs concentration (Figure 1j). Such results indicate that the enhancement in MWCNT retention due to the presence of GNPs is still limited. A more negative value of $R_{M/S}$ for GNPs in comparison to BNPs (Figure 1k) indicates that the inhibitory effect on MWCNT retention was more pronounced for GNP than BNP.

Potential Mechanisms Contributing to the Retention of MWCNTs. Previous studies indicated that the co-transport of ENPs and SNPs may occur via the following mechanisms:[22,64] (i) competitive blocking due to limited retention sites; (ii) heteroaggregation; and (iii) interaction between these colloids and porous media. Each of these factors is discussed below.

Competitive Blocking. Blocking (increasing effluent concentrations with continued particle injection) occurs for MWCNTs, BNPs, and GNPs (Figure 1). Increasing the SNPs C_o will also decrease S_S^{max}/C_o and thereby enhance blocking (sites fill faster at higher C_o). When competitive blocking is considered, the retention of SNPs will also contribute to the filling of the MWCNT S_M^{max}. Numerical simulations exploring the significance of competitive blocking were conducted by implementing the M1 and M2 modules, respectively (Figure S3 and Table 2). Better simulation results (Figure S3 and Table 2) were achieved while using the M2 module and both Γ_M and Γ_S were greater than 0, suggesting that competitive blocking should play a role in the co-transport of MWCNT and SNPs. However, one should note that the fitted values of Γ_M and Γ_S for the co-transport experiments were low, indicating that competitive blocking is likely not the dominant contributor to co-transport enhancement (MWCNTs and BNPs) or inhibition (MWCNTs in the presence of GNPs).

Heteroaggregation. Some recent studies suggested that heteroaggregation could occur between ENPs and clay minerals or iron oxides due to electrical interaction, cation bridges, hydrogen bonding, and other interactions.[65−69] Our previous studies have shown that MWCNTs (1 mg L^{-1}) in 1 mM KCl suspension are stable within 4 h in the absence of BNPs and GNPs.[36] MWCNT suspensions exhibited larger hydrodynamic radii after adding BNPs or GNPs that were stable for at least 1 h after preparation (Table S1). Such results suggested that heteroaggregation (MWCNTs-BNPs and MWCNTs-GNPs) occurred during the co-transport of MWCNTs and SNPs (BNPs or GNPs) in porous media.

AF4-UV-ICP-MS has been used to study the interactions of soil elements (*e.g.*, phosphorus) with soil colloids and nanoparticles.[70−72] In this research, AF4-UV-ICP-MS was used for the first time to characterize the association between ENPs and SNPs in the effluent of co-transport experiments. This method allows us to distinguish homo- and hetero-aggregates of nanoparticles and colloids in suspension. Figure 2a,c shows the UV fractograms (volts) for MWCNTs-BNPs and MWCNTs-GNPs, respectively, in the column effluent. Figure 2b,d provides the corresponding plots of the ICP-MS concentration (μg L^{-1}) of particulate Al (for BNPs) and Fe (for GNPs), respectively, in effluent samples with the corresponding hydrodynamic radius (nm). Extremely low particulate Al and Fe concentrations were detected with pure MWCNTs in the absence of SNPs (Figure 2b–d, black line, 1 mg L^{-1}), indicating only minor traces of catalyst in MWCNTs.[61] The MWCNTs fractogram indicated two different size ranges: 1–20 and 125–200 nm in both UV and ICP-MS measurements (Figure 2a–d).[73] Conversely,

https://doi.org/10.1021/acs.est.2c00681
Environ. Sci. Technol. XXXX, XXX, XXX−XXX

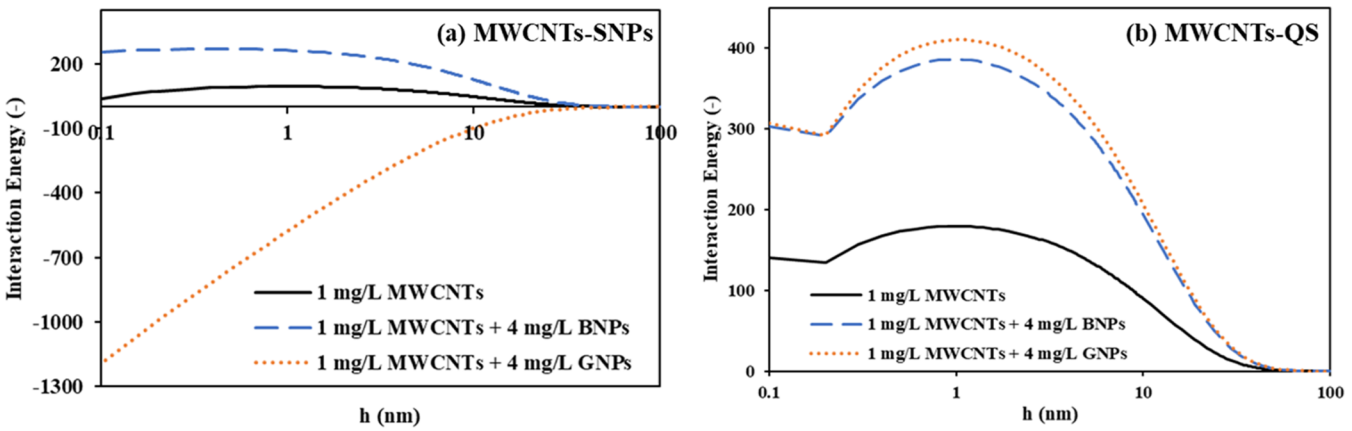

Figure 3. Plots of the dimensionless interaction energy as a function of separation distance (h) when a spherical colloid, with properties similar to MWCNTs at an ionic strength of 1 mM KCl in the presence or absence of SNPs (BNPs or GNPs) (a), and in QS in the presence or absence of SNPs (BNPs or GNPs) (b), respectively; (a) 1 mg L^{-1} MWCNT with adding 0 and 4 mg L^{-1} of SNPs (BNPs or GNPs); (b) 1 mg L^{-1} MWCNT with adding 0 and 4 mg L^{-1} of SNPs (BNPs or GNPs) in QS.

much higher UV intensities and particulate Al and Fe concentrations were observed in the effluent of co-transport experiments when SNPs were present. Larger particles, especially in the range of 125−200 nm, were found in the effluent of co-transport experiments when SNPs were present, and their composition was indicative of the presence of heteroaggregates. TEM images were obtained for effluent samples under different conditions (Figure S1c,d for BNPs, and Figure S1e,f for GNPs) for further confirmation. It was found that MWCNTs have interacted with BNPs and GNPs (red circle) in the effluent. These findings indicate that BNPs and GNPs were associated with MWCNTs under the tested conditions.

Batch experiments with AF4-UV-ICP-MS measurements were conducted to improve our understanding of the association between MWCNTs and BNPs or GNPs. Batch results indicate that both BNPs and GNPs can adsorb MWCNTs, but there were stronger affinities between MWCNTs-GNPs than MWCNTs-BNPs (Figure S4). The AF4-UV-ICP-MS results showed larger MWCNT-BNP and MWCNT-GNP aggregates in batch than column experiments. One potential explanation is that larger-sized aggregates were retained in the QS during the co-transport of MWCNTs and SNPs, and only smaller-sized aggregates were observed in the effluent. Overall, AF4-UV-ICP-MS results from both column and batch experiments indicated that MWCNTs-BNPs or MWCNT-GNPs heteroaggregates were formed during co-transport.

Interactions. DLVO calculations are normally conducted to explain observed aggregation and retention behavior. Figure 3a presents plots of Φ as a function of separation distance (h) when a spherical colloid with properties similar to MWCNTs approaches a spherical colloid with properties similar to BNPs or GNPs in KCl solutions at IS = 1 mM. A large energy barrier is predicted between MWCNTs and MWCNTs-BNPs, whereas there is no energy barrier between MWCNTs-GNPs. Figure 3b presents similar information for a spherical MWCNT colloid as it approaches the surface of QS in KCl solutions at IS = 1 mM. A large energy barrier and a shallow secondary minimum are predicted between the MWCNTs and QS, although the height of the energy barrier and the depth of the primary minimum is a function of the various concentrations of BNPs or GNPs (Figure S5) because of their influence on ζ-potentials (Figure S6); e.g., the ζ-potential of MWCNTs was more negative in the presence of BNPs (−40.9 and −41.4 mV for 4 and 10 mg L^{-1} BNPs, respectively) and less negative in the presence of GNPs (−38.7 and −36.4 mV for 2 and 4 mg L^{-1} GNPs, respectively) in comparison to MWCNT suspensions without SNPs (−40.6 mV, Figure S6).

Although DLVO calculations in Figure 3 can explain the association of MWCNTs with GNPs, it cannot account for associations between MWCNT and BNPs, the significant amount of MWCNT retention, and competitive blocking. Other forces and factors may therefore be required to explain this behavior. For example, calculations in Figure 3 assume smooth and chemically homogeneous surfaces, whereas surface roughness and charge heterogeneity on natural surfaces or due to attached SNPs will locally reduce or eliminate the energy barrier.[74,75] Furthermore, MWCNTs are not spherical in shape, and the particle shape, orientation with the surface, and the interior properties are known to have a strong impact on predicted energy barriers.[76−78] If these factors eliminate the energy barrier, then the MWCNTs can interact in a primary minimum at a small separation distance and other non-DLVO forces can contribute to the strength of the interaction.[26,27]

The FTIR spectra from batch experiments (Figures 2 and S7) showed O−H stretching (3437.4 cm^{-1}), weak C−H stretching (2918.4 cm^{-1}) of $-CH_3$ and CH_2 groups, carboxylic C═O (1726.9 cm^{-1}) and COO^- (1575.3 cm^{-1}) stretching, and C−O stretching (1152.4 cm^{-1}) from functionalized MWCNTs.[79−81] A new band appeared at 1405.9 cm^{-1} (Figure 2f) in comparison to the pristine GNPs, which was induced by the complexation between GNPs and the COO^- groups of MWCNTs. Similar results have been observed for the association of organic matter with iron oxide.[27,82−84] In addition, a small decrease in intensity of the band below 1000.0 cm^{-1} (607.7, 801.2, and 909.6 cm^{-1}, Fe−O or Fe−OH vibrations) and 3130.7 cm^{-1} (O−H stretching), as well as a disappearance in the intensity of the band around 1060.0 cm^{-1} (Fe−OH vibration), were attributed to the association between water or Fe−OH or Fe−O vibrations of GNPs and MWCNTs by non-DLVO interactions (e.g., H-bonding, Lewis acid−base, or ligand exchange).[26,82−84] Figure 2e shows the association between BNPs and MWCNTs, which exhibited much weaker complexing ability in comparison to MWCNTs

https://doi.org/10.1021/acs.est.2c00681
Environ. Sci. Technol. XXXX, XXX, XXX−XXX

and GNPs. Only a slight decrease in intensity of the band around 467.9 (Si−O vibration), 525.0 (Si−O vibration), 3440.1 (O−H stretching), and 3621.6 (O−H stretching) cm^{-1} was found, suggesting the interaction between MWCNTs and BNPs through water molecular and Si−O vibrations on BNPs.

The FTIR results provided qualitative information regarding the interactions and indicated that the interactions between MWCNTs (negatively charged) and SNPs (negatively charged BNPs or positively charged GNPs, Figure 2e,f) are also through non-DLVO interactions with functional groups of Si−O on BNP surfaces or Fe−O and/or Fe−OH on the GNP surfaces, and −COOH and/or −OH on MWCNT surfaces. Only a few studies based on batch and aggregation experiments have shown that carbon nanomaterials can interact with goethite through H-bonding and/or Lewis acid−base interactions at both negatively and positively charged goethite, and further indicated that both H-bonding and Lewis acid−base interactions may overcome the electrostatic repulsion between them.[26,27] Consequently, results herein demonstrated that both BNPs and GNPs could interact with MWCNTs through non-DLVO interactions (e.g., H-bonding, Lewis acid−base interactions, or ligand exchange).

Theoretical calculations evaluating the binding energies between MWCNTs and SNPs were performed by conducting MD simulations (Figure 4). The binding energies of BNPs (Figure 4b) and GNPs (Figure 4c) with MWCNTs were −120.6 ± −7.6 and −175.3 ± −8.6 kJ mol^{-1}, which is equivalent to −48.7 and −70.68 kT (1 kT = 2.476 kJ mol^{-1}),[85] respectively. These attractive interactions are much stronger than expected for secondary minimum interactions and are much shallower than primary minimum interactions on smooth surfaces. However, their magnitudes are comparable to primary minimum interactions when surface roughness and charge heterogeneities are considered for MWCNTs and SNPs (Figure S5c,d).

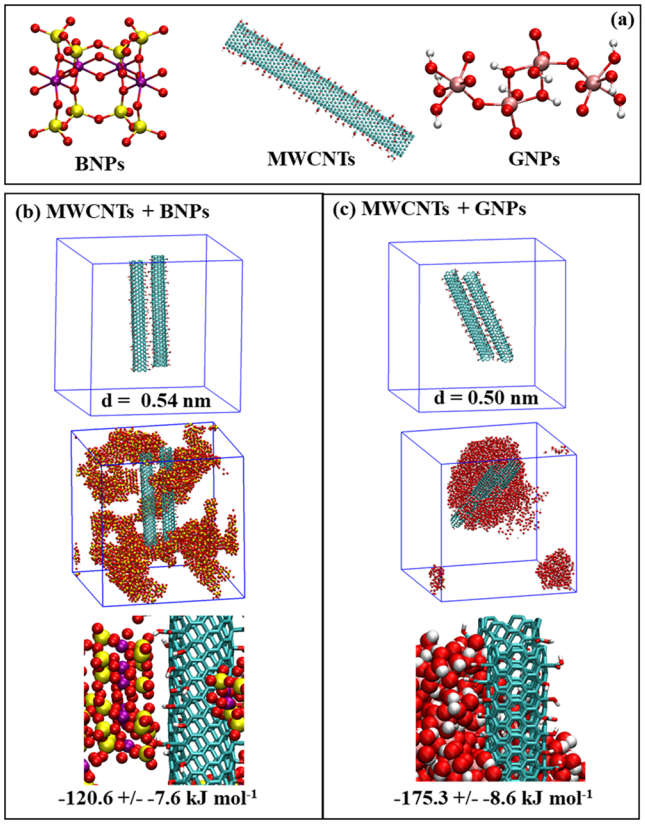

Figure 4. (a−c) MD simulations of MWCNTs with BNPs or GNPs. (a) Schematic molecular structure for BNPs, MWCNTs, and GNPs. Red is oxygen (O), white is hydrogen (H), light blue is carbon (C), light pink is iron (Fe), yellow is silicon (Si), and purple is aluminum (Al). The solvent of KCl and water molecular has been hidden for a better observation. (b, c) Interactions between MWCNTs and BNPs, and MWCNTs and GNPs, respectively; *d* is the mean distance between the centroids of two MWCNTs.

In addition, MD simulations show that MWCNTs can be completely wrapped by GNPs with a smaller mean distance (0.50 nm, Figure 4c) between the centroids of MWCNTs. Although MWCNTs were also wrapped by BNPs, much greater dispersion around MWCNTs than GNPs was observed, resulting in a larger mean distance (0.54 nm, Figure 4b) between the centroids of MWCNTs. The tiny difference of 0.50 and 0.54 nm still exhibited the effect of interactions between MWCNTs and SNPs, which were in good agreement with the observation of enhanced hydrodynamic radii of MWCNTs found in the presence of GNPs and BNPs (Table S1) and results of AF4-UV-ICP-MS.

Our MD simulations demonstrate that non-DLVO interactions between SNP and MWCNT are thermodynamically feasible, so their contributions to the deposition and interaction behavior of SNPs and MWCNTs should not be ignored. FTIR results (Figure 2e,f) experimentally confirm these findings. Non-DLVO interactions like chemical and H-bonding should make MWCNTs-SNPs aggregates that are more stable than those predicted by conventional DLVO theory, and consequently less susceptible to disaggregation.

Other than the commonly observed facilitated transport behavior, we for the first time found that the transport of both BNPs and GNPs was also facilitated by the presence of MWCNTs. Such phenomena cannot be effectively explained by the traditional mechanisms associated with competitive blocking, heteroaggregation, and conventional DLVO calculations. Direct examination using novel tools of AF4-UV-ICP-MS measurement combined with MD simulation, batch experiments, and FTIR measurement collectively demonstrated that MWCNTs-BNPs or MWCNTs-GNPs complexes or aggregates could be formed and non-DLVO interactions (e.g., H-bonding, Lewis acid−base interactions, or ligand exchange) played an important role in contributing to the co-transport between SNPs (BNPs or GNPs) and MWCNTs. An input concentration of 1 mg L^{-1} of MWCNTs was employed to obtain high accuracy and mass balance in studies designed to evaluate heteroaggregation and co-transport of ENPs and SNPs in soil, although this value is high in comparison to environmentally relevant MWCNT concentrations that were modeled or estimated by other studies.[86,87] Consequently, the mutual effects (enhancement or inhibition) of two colloids in co-transport should be considered in soil and groundwater.

■ ENVIRONMENTAL IMPLICATIONS

Soil nanoparticles (SNPs) are one of the most active components involved in many biogeochemical processes in soil and groundwater. In this work, a multiscale approach was employed to comprehensively evaluate the contributions of negatively and positively charged SNPs (BNPs and GNPs) to the transport and retention of MWCNTs in QS. The results demonstrated that the mutual effects of MWCNTs and SNPs (BNPs or GNPs) could not be well described by classic DLVO

https://doi.org/10.1021/acs.est.2c00681
Environ. Sci. Technol. XXXX, XXX, XXX−XXX

theory, CFT, and competitive blocking due to the contributions of non-DLVO interactions to aggregation and co-transport of MWCNTs and SNPs. In natural soil and groundwater environments, co-transport, heteroaggregation, or interactions of MWCNTs can occur with SNPs and colloids regardless of the surface charge of particles and the collector (similarly or oppositely charged). Some colloidal contaminants or other colloids with oxygen-containing functional groups like functionalized MWCNTs, biochar, or biocolloids can interact with colloids and SNPs through non-DLVO interactions in soil and groundwater. Future research should accurately quantify (*e.g.*, MD simulation, atomic force microscopy (AFM), density functional theory (DFT), etc.) the contribution of non-DLVO interactions (e.g., H-bonding, Lewis acid−base interactions, or ligand exchange) to colloids and SNPs (*e.g.*, heteroaggregation and co-transport) in the environment. In fact, homo- and heteroaggregates in suspension can be distinguished by AF4-UV-DLS-ICP-MS by determining changes in size fraction and element composition. Single-particle ICP-MS also helps to identify and quantify the low concentrations and size of ENPs in the environment[45−47] and possibly ENPs-SNPs aggregates in the future.[88] The interfacial forces between colloids and collectors could be directly determined by AFM.[89] Both MD simulation and DFT could provide the interaction mechanism between molecules or/and atoms.[35,90] Consequently, the role of non-DLVO interactions should be comprehensively evaluated and further investigated when assessing the environmental risk and fate of ENPs or colloidal contaminants (*e.g.*, coexistence of multisubstance) that are associated with soil colloids/SNPs.

■ ASSOCIATED CONTENT

Supporting Information

The Supporting Information is available free of charge at https://pubs.acs.org/doi/10.1021/acs.est.2c00681.

Details pertaining to BNPs and GNPs preparation (S1), interaction energy calculations (S2), batch experiments (S3), and numerical modeling (S4); hydrodynamic radii of MWCNTs, BNPs, GNPs, BNPs-MWCNTs, and GNPs-MWCNTs at 1 mM KCl (Table S1); fitted parameters based on M1 and M2 models (Table S2); scanning electron microscope images of BNPs and GNPs, and transmission electron microscopy images of BNPs-MWCNTs and GNPs-MWCNTs in the effluent of column experiments (Figure S1); AF4 fractograms of BNPs and GNPs suspensions (4 mg L^{-1} BNPs or GNPs, 1 mM KCl) (Figure S2); observed and fitted (M2 model) BTCs and RPs in the column experiments (Figure S3); results of a batch experiment on the attachment of MWCNTs to BNPs or GNPs in 1 mM KCl solution (Figure S4); interaction energies between MWCNTs and QS in the presence or absence of SNPs (BNPs or GNPs) under different roughness conditions (Figure S5); ζ-potentials of MWCNTs, BNPs, GNPs, BNPs-MWCNT, and GNPs-MWCNTs at the ionic strength of 1 mM KCl (pH ≈ 5.4) (Figure S6); and FTIR spectra of MWCNTs (Figure S7) (PDF)

■ AUTHOR INFORMATION

Corresponding Author

Chao Jin − *School of Environmental Science and Engineering, Sun Yat-sen University, Guangzhou 510006, P. R. China; Guangdong Provincial Key Laboratory of Environmental Pollution Control and Remediation Technology, Sun Yat-sen University, Guangzhou 510006, P. R. China;* orcid.org/0000-0001-6590-333X; Phone: 86-20-39335060; Email: jinchao3@mail.sysu.edu.cn

Authors

Miaoyue Zhang − *School of Environmental Science and Engineering, Sun Yat-sen University, Guangzhou 510006, P. R. China; Guangdong Provincial Key Laboratory of Environmental Pollution Control and Remediation Technology, Sun Yat-sen University, Guangzhou 510006, P. R. China;* orcid.org/0000-0002-2939-6665

Scott A. Bradford − *Sustainable Agricultural Water Systems (SAWS) Unit, USDA, ARS, UC Davis, Davis, California 95616, United States;* orcid.org/0000-0002-3260-2968

Erwin Klumpp − *Agrosphere Institute (IBG-3), Forschungszentrum Jülich GmbH, 52425 Jülich, Germany*

Jiri Šimůnek − *Department of Environmental Sciences, University of California, Riverside, Riverside, California 92521, United States*

Shizhong Wang − *School of Environmental Science and Engineering, Sun Yat-sen University, Guangzhou 510006, P. R. China; Guangdong Provincial Key Laboratory of Environmental Pollution Control and Remediation Technology, Sun Yat-sen University, Guangzhou 510006, P. R. China*

Quan Wan − *Guangdong Provincial Key Laboratory of Agricultural & Rural Pollution Abatement and Environmental Safety, College of Natural Resources and Environment, South China Agricultural University, Guangzhou 510642, P. R. China*

Rongliang Qiu − *School of Environmental Science and Engineering, Sun Yat-sen University, Guangzhou 510006, P. R. China; Guangdong Provincial Key Laboratory of Agricultural & Rural Pollution Abatement and Environmental Safety, College of Natural Resources and Environment, South China Agricultural University, Guangzhou 510642, P. R. China; Guangdong Laboratory for Lingnan Modern Agriculture, Guangzhou 510642, P. R. China;* orcid.org/0000-0002-9469-5274

Complete contact information is available at: https://pubs.acs.org/10.1021/acs.est.2c00681

Notes

The authors declare no competing financial interest.

■ ACKNOWLEDGMENTS

Funding was provided by the National Natural Science Foundation of China (project nos. 42077342 and 41877475) and the 111 Project (project no. B18060). The authors acknowledge Stephan Köppchen for bromide measurements. Thanks go to Herbert Philipp and Claudia Walraf for their technical assistance.

■ REFERENCES

(1) Iijima, S. Helical Microtubules of Graphitic Carbon. *Nature* **1991**, *354*, 56−58.

(2) Camilli, L.; Pisani, C.; Gautron, E.; Scarselli, M.; Castrucci, P.; D'Orazio, F.; Passacantando, M.; Moscone, D.; De Crescenzi, M. A Three-Dimensional Carbon Nanotube Network for Water Treatment. *Nanotechnology* **2014**, *25*, No. 065701.

(3) Zhang, S.; Shao, T.; Kose, H. S.; Karanfil, T. Adsorption of Aromatic Compounds by Carbonaceous Adsorbents: A Comparative Study on Granular Activated Carbon, Activated Carbon Fiber, and Carbon Nanotubes. *Environ. Sci. Technol.* **2010**, *44*, 6377−6383.
(4) Pan, B.; Xing, B. Applications and Implications of Manufactured Nanoparticles in Soils: A Review. *Eur. J. Soil Sci.* **2012**, *63*, 437−456.
(5) Mauter, M. S.; Elimelech, M. Environmental Applications of Carbon-Based Nanomaterials. *Environ. Sci. Technol.* **2008**, *42*, 5843−5859.
(6) Li, C.; Schäffer, A.; Séquaris, J.-M.; László, K.; Tóth, A.; Tombácz, E.; Vereecken, H.; Ji, R.; Klumpp, E. Surface-Associated Metal Catalyst Enhances the Sorption of Perfluorooctanoic Acid to Multi-Walled Carbon Nanotubes. *J. Colloid Interface Sci.* **2012**, *377*, 342−346.
(7) Lowry, G. V.; Gregory, K. B.; Apte, S. C.; Lead, J. R. Transformations of Nanomaterials in the Environment. *Environ. Sci. Technol.* **2012**, *46*, 6893−6899.
(8) Kasel, D.; Bradford, S. A.; Šimůnek, J.; Pütz, T.; Vereecken, H.; Klumpp, E. Limited Transport of Functionalized Multi-Walled Carbon Nanotubes in Two Natural Soils. *Environ. Pollut.* **2013**, *180*, 152−158.
(9) Tian, Y.; Gao, B.; Wu, L.; Munoz-Carpena, R.; Huang, Q. Effect of Solution Chemistry on Multi-Walled Carbon Nanotube Deposition and Mobilization in Clean Porous Media. *J. Hazard. Mater.* **2012**, *231*−*232*, 79−87.
(10) Yang, J.; Bitter, J. L.; Smith, B. A.; Fairbrother, D. H.; Ball, W. P. Transport of Oxidized Multi-Walled Carbon Nanotubes through Silica Based Porous Media: Influences of Aquatic Chemistry, Surface Chemistry, and Natural Organic Matter. *Environ. Sci. Technol.* **2013**, *47*, 14034−14043.
(11) Zhang, M.; Bradford, S. A.; Šimůnek, J.; Vereecken, H.; Klumpp, E. Co-Transport of Multi-Walled Carbon Nanotubes and Sodium Dodecylbenzenesulfonate in Chemically Heterogeneous Porous Media. *Environ. Pollut.* **2019**, *247*, 907−916.
(12) Zhang, M.; Engelhardt, I.; Šimůnek, J.; Bradford, S. A.; Kasel, D.; Berns, A. E.; Vereecken, H.; Klumpp, E. Co-Transport of Chlordecone and Sulfadiazine in the Presence of Functionalized Multi-Walled Carbon Nanotubes in Soils. *Environ. Pollut.* **2017**, *221*, 470−479.
(13) Kasel, D.; Bradford, S. A.; Šimůnek, J.; Heggen, M.; Vereecken, H.; Klumpp, E. Transport and Retention of Multi-Walled Carbon Nanotubes in Saturated Porous Media: Effects of Input Concentration and Grain Size. *Water Res.* **2013**, *47*, 933.
(14) Hochella, M. F.; Mogk, D. W.; Ranville, J.; Allen, I. C.; Luther, G. W.; Marr, L. C.; McGrail, B. P.; Murayama, M.; Qafoku, N. P.; Rosso, K. M.; Sahai, N.; Schroeder, P. A.; Vikesland, P.; Westerhoff, P.; Yang, Y. Natural, Incidental, and Engineered Nanomaterials and Their Impacts on the Earth System. *Science* **2019**, *363*, No. eaau8299.
(15) Barnard, A. S.; Guo, H. *Nature's Nanostructures*; Pan Stanford Publishing: Singapore, 2012.
(16) Theng, B. K. G.; Yuan, G. Nanoparticles in the Soil Environment. *Elements* **2008**, *4*, 395−399.
(17) Cai, L.; Meiping, T.; Xueting, W.; Hyunjung, K. Influence of Clay Particles on the Transport and Retention of Titanium Dioxide Nanoparticles in Quartz Sand. *Environ. Sci. Technol.* **2014**, *48*, 7323−7332.
(18) Yang, H.; Ge, Z.; Wu, D.; Tong, M.; Ni, J. Cotransport of Bacteria with Hematite in Porous Media: Effects of Ion Valence and Humic Acid. *Water Res.* **2016**, *88*, 586−594.
(19) Syngouna, V. I.; Chrysikopoulos, C. V. Cotransport of Clay Colloids and Viruses through Water-Saturated Vertically Oriented Columns Packed with Glass Beads: Gravity Effects. *Sci. Total Environ.* **2016**, *545*−*546*, 210−218.
(20) Katzourakis, V. E.; Chrysikopoulos, C. V. Mathematical Modeling of Colloid and Virus Cotransport in Porous Media: Application to Experimental Data. *Adv. Water Resour.* **2014**, *68*, 62−73.
(21) Katzourakis, V. E.; Chrysikopoulos, C. V. Modeling Dense-Colloid and Virus Cotransport in Three-Dimensional Porous Media. *J. Contam. Hydrol.* **2015**, *181*, 102−113.
(22) Li, M.; He, L.; Zhang, M.; Liu, X.; Tong, M.; Kim, H. Cotransport and Deposition of Iron Oxides with Different Sized-Plastic Particles in Saturated Quartz Sand. *Environ. Sci. Technol.* **2019**, *53*, 3547−3557.
(23) Dong, Z.; Zhang, W.; Qiu, Y.; Yang, Z.; Wang, J.; Zhang, Y. Cotransport of Nanoplastics (NPs) with Fullerene (C_{60}) in Saturated Sand: Effect of NPs/C_{60} Ratio and Seawater Salinity. *Water Res.* **2019**, *148*, 469−478.
(24) Liu, J.; Legros, S.; von der Kammer, F.; Hofmann, T. Natural Organic Matter Concentration and Hydrochemistry Influence Aggregation Kinetics of Functionalized Engineered Nanoparticles. *Environ. Sci. Technol.* **2013**, *47*, 4113−4120.
(25) Yecheskel, Y.; Dror, I.; Berkowitz, B. Effect of Phosphate, Sulfate, Arsenate, and Pyrite on Surface Transformations and Chemical Retention of Gold Nanoparticles (Au−NPs) in Partially Saturated Soil Columns. *Environ. Sci. Technol.* **2019**, *53*, 13071−13080.
(26) Lian, F.; Yu, W.; Wang, Z.; Xing, B. New Insights into Black Carbon Nanoparticle-Induced Dispersibility of Goethite Colloids and Configuration-Dependent Sorption for Phenanthrene. *Environ. Sci. Technol.* **2019**, *53*, 661−670.
(27) Liu, X.; Li, J.; Huang, Y.; Wang, X.; Zhang, X.; Wang, X. Adsorption, Aggregation, and Deposition Behaviors of Carbon Dots on Minerals. *Environ. Sci. Technol.* **2017**, *51*, 6156−6164.
(28) Yang, F.; Xu, Z.; Huang, Y.; Tsand, D. C. W.; Yong, S. O.; Zhao, L.; Qiu, H.; Xu, X.; Cao, X. Stabilization of Dissolvable Biochar by Soil Minerals: Release Reduction and Organo-Mineral Complexes Formation. *J. Hazard. Mater.* **2021**, *412*, No. 125213.
(29) Chrysikopoulos, C. V.; Sotirelis, N. P.; Kallithrakas-Kontos, N. G. Cotransport of Graphene Oxide Nanoparticles and Kaolinite Colloids in Porous Media. *Transp. Porous Med.* **2017**, *119*, 181−204.
(30) Cai, L.; Tong, M.; Wang, X.; Kim, H. Influence of Clay Particles on the Transport and Retention of Titanium Dioxide Nanoparticles in Quartz Sand. *Environ. Sci. Technol.* **2014**, *48*, 7323−7332.
(31) He, L.; Wu, D.; Rong, H.; Li, M.; Tong, M.; Kim, H. Influence of Nano- and Microplastic Particles on the Transport and Deposition Behaviors of Bacteria in Quartz Sand. *Environ. Sci. Technol.* **2018**, *52*, 11555−11563.
(32) Bayat, A. E.; Junin, R.; Mohsin, R.; Hokmabadi, M.; Shamshirband, S. Influence of Clay Particles on Al_2O_3 and TiO_2 Nanoparticles Transport and Retention through Limestone Porous Media: Measurements and Mechanisms. *J. Nanopart. Res.* **2015**, *17*, 219.
(33) Katzourakis, V. E.; Chrysikopoulos, C. V. Modeling the Transport of Aggregating Nanoparticles in Porous Media. *Water Resour. Res.* **2020**, *57*, No. e2020WR027946.
(34) Zhao, J.; Liu, F.; Wang, Z.; Cao, X.; Xing, B. Heteroaggregation of Graphene Oxide with Minerals in Aqueous Phase. *Environ. Sci. Technol.* **2015**, *49*, 2849−2857.
(35) Zhang, M.; Bradford, S. A.; Klumpp, E.; Šimůnek, J.; Qiu, R. Non-Monotonic Contribution of Nonionic Surfactant on the Retention of Functionalized Multi-Walled Carbon Nanotubes in Porous Media. *J. Hazard. Mater.* **2020**, *407*, No. 124874.
(36) Zhang, M.; Bradford, S. A.; Šimůnek, J.; Vereecken, H.; Klumpp, E. Roles of Cation Valance and Exchange on the Retention and Colloid-Facilitated Transport of Functionalized Multi-Walled Carbon Nanotubes in a Natural Soil. *Water Res.* **2017**, *109*, 358.
(37) Israelachvili, J. N. Special Interactions: Hydrogen-Bonding and Hydrophobic and Hydrophilic Interactions. In *Intermolecular and Surface Forces*, 3rd ed.; Israelachvili, J. N., Ed.; Academic Press: Boston, 2011; pp 151−167.
(38) Pauluhn, J. Multi-Walled Carbon Nanotubes (Baytubes): Approach for Derivation of Occupational Exposure Limit. *Regul. Toxicol. Pharmacol.* **2010**, *57*, 78−89.

https://doi.org/10.1021/acs.est.2c00681
Environ. Sci. Technol. XXXX, XXX, XXX−XXX

(39) Pecora, R. Dynamic Light Scattering Measurement of Nanometer Particles in Liquids. *J. Nanopart. Res.* **2000**, *2*, 123−131.
(40) Hassellöv, M.; Readman, J. W.; Ranville, J. F.; Tiede, K. Nanoparticle Analysis and Characterization Methodologies in Environmental Risk Assessment of Engineered Nanoparticles. *Ecotoxicology* **2008**, *17*, 344−361.
(41) Bradford, S. A.; Torkzaban, S. Colloid Interaction Energies for Physically and Chemically Heterogeneous Porous Media. *Langmuir* **2013**, *29*, 3668−3676.
(42) Test No. 106: Adsorption − Desorption Using a Batch Equilibrium Method. In *OECD Guidelines for the Testing of Chemicals*, OECD, 2006; Vol. *1*, pp 1−44.
(43) Zhang, M.; Bradford, S. A.; Šimůnek, J.; Vereecken, H.; Klumpp, E. Do Goethite Surfaces Really Control the Transport and Retention of Multi-Walled Carbon Nanotubes in Chemically Heterogeneous Porous Media? *Environ. Sci. Technol.* **2016**, *50*, 12713.
(44) Abraham, P. M.; Barnikol, S.; Baumann, T.; Kuehn, M.; Ivleva, N. P.; Schaumann, G. Sorption of Silver Nanoparticles to Environmental and Model Surfaces. *Environ. Sci. Technol.* **2013**, *47*, 5083−5091.
(45) Wang, J.; Nabi, M. M.; Erfani, M.; Goharian, E.; Baalousha, M. Identification and Quantification of Anthropogenic Nanomaterials in Urban Rain and Runoff Using Single Particle-Inductively Coupled Plasma-Time of Flight-Mass Spectrometry. *Environ. Sci.: Nano* **2022**, *9*, 714−729.
(46) Baalousha, M.; Wang, J.; Erfani, M.; Goharian, E. Elemental Fingerprints in Natural Nanomaterials Determined Using SP-ICP-TOF-MS and Clustering Analysis. *Sci. Total Environ.* **2021**, *792*, No. 148426.
(47) Bland, G. D.; Battifarano, M.; Pradas del Real, A. E.; Sarret, G.; Lowry, G. V. Distinguishing Engineered TiO_2 Nanomaterials from Natural Ti Nanomaterials in Soil Using Spicp-Tofms and Machine Learning. *Environ. Sci. Technol.* **2022**, *56*, 2990−3001.
(48) Šimůnek, J.; Genuchten, M. T. V.; Šejna, M. Development and Applications of the Hydrus and Stanmod Software Packages and Related Codes. *Vadose Zone J.* **2008**, *7*, 587−600.
(49) Bradford, S. A.; Leij, F. J. Modeling the Transport and Retention of Polydispersed Colloidal Suspensions in Porous Media. *Chem. Eng. Sci.* **2018**, *192*, 972−980.
(50) Šimůnek, J.; He, C.; Pang, L.; Bradford, S. A. Colloid-Facilitated Solute Transport in Variably Saturated Porous Media. *Vadose Zone J.* **2006**, *5*, 1035−1047.
(51) Akaike, H. A New Look at the Statistical Model Identification. *IEEE Trans. Autom. Control* **1974**, *19*, 716−723.
(52) Missong, A.; Holzmann, S.; Bol, R.; Nischwitz, V.; Puhlmann, H.; v Wilpert, K.; Siemens, J.; Klumpp, E. Leaching of Natural Colloids from Forest Topsoils and Their Relevance for Phosphorus Mobility. *Sci. Total Environ.* **2018**, *634*, 305−315.
(53) Makselon, J.; Siebers, N.; Meier, F.; Vereecken, H.; Klumpp, E. Role of Rain Intensity and Soil Colloids in the Retention of Surfactant-Stabilized Silver Nanoparticles in Soil. *Environ. Pollut.* **2018**, *238*, 1027−1034.
(54) Vanommeslaeghe, K.; Hatcher, E.; Acharya, C.; Kundu, S.; Zhong, S.; Shim, J.; Darian, E.; Guvench, O.; Lopes, P.; Vorobyov, I.; MacKerell, A. D., Jr. Charmm General Force Field: A Force Field for Drug-Like Molecules Compatible with the Charmm All-Atom Additive Biological Force Fields. *J. Comput. Chem.* **2010**, *31*, 671−690.
(55) Gutiérrez, I. S.; Lin, F. Y.; Vanommeslaeghe, K.; Lemkul, J. A.; Armacost, K. A.; Brooks, C. L.; MacKerell, A. D., Jr. Parametrization of Halogen Bonds in the Charmm General Force Field: Improved Treatment of Ligand−Protein Interactions. *Bioorg. Med. Chem.* **2016**, *24*, 4812−4825.
(56) Polyakov, I.; Epifanovsky, E.; Krylov, A. I.; Nemukhin, A. V.; Guidoni, L. Quantum Chemical Benchmark Studies of the Electronic Properties of the Green Fluorescent Protein Chromophore: 2. Cis-Trans Isomerization in Water. *J. Chem. Theory Comput.* **2009**, *5*, 1907−1914.
(57) Berendsen, H. J. C. P.; Postma, J.; Gunsteren, W.; Dinola, A. D.; Haak, J. R. Molecular-Dynamics with Coupling to an External Bath. *J. Chem. Phys.* **1984**, *81*, 3684.
(58) Essmann, U.; Perera, L.; Berkowitz, M. L.; Darden, T.; Lee, H.; Pedersen, L. G. A Smooth Particle Mesh Ewald Method. *J. Chem. Phys.* **1995**, *103*, 8577−8593.
(59) Astrakas, L. G.; Gousias, C.; Tzaphlidou, M. Structural Destabilization of Chignolin under the Influence of Oscillating Electric Fields. *J. Appl. Phys.* **2012**, *111*, No. 074702.
(60) Hess, B.; Bekker, H.; Berendsen, H. J. C.; Fraaije, J. G. E. M. LINCS: A Linear Constraint Solver for Molecular Simulations. *J. Comput. Chem.* **1997**, *18*, 1463−1472.
(61) Kasel, D.; Bradford, S. A.; Šimůnek, J.; Heggen, M.; Vereecken, H.; Klumpp, E. Transport and Retention of Multi-Walled Carbon Nanotubes in Saturated Porous Media: Effects of Input Concentration and Grain Size. *Water Res.* **2013**, *47*, 933−944.
(62) Jaisi, D. P.; Saleh, N. B.; Blake, R. E.; Elimelech, M. Transport of Single-Walled Carbon Nanotubes in Porous Media: Filtration Mechanisms and Reversibility. *Environ. Sci. Technol.* **2008**, *42*, 8317−8323.
(63) Wang, Y.; Kim, J. H.; Baek, J. B.; Miller, G. W.; Pennell, K. D. Transport Behavior of Functionalized Multi-Wall Carbon Nanotubes in Water-Saturated Quartz Sand as a Function of Tube Length. *Water Res.* **2012**, *46*, 4521−4531.
(64) Yang, H.; Ge, Z.; Dan, W.; Tong, M.; Ni, J. Cotransport of Bacteria with Hematite in Porous Media: Effects of Ion Valence and Humic Acid. *Water Res.* **2016**, *88*, 586−594.
(65) Lenhart, J. J.; Yu, S. H.; Liu, J. Heteroaggregation of Bare Silver Nanoparticles with Clay Minerals. *Environ. Sci.: Nano* **2015**, *2*, 528−540.
(66) Wang, H.; Adeleye, A. S.; Huang, Y.; Li, F.; Keller, A. A. Heteroaggregation of Nanoparticles with Biocolloids and Geocolloids. *Adv. Colloid Interface Sci.* **2015**, *226*, 24−36.
(67) Labille, J.; Harns, C.; Bottero, J.-Y.; Brant, J. Heteroaggregation of Titanium Dioxide Nanoparticles with Natural Clay Colloids. *Environ. Sci. Technol.* **2015**, *49*, 6608−6616.
(68) Huynh, K. A.; McCaffery, J. M.; Chen, K. L. Heteroaggregation of Multiwalled Carbon Nanotubes and Hematite Nanoparticles: Rates and Mechanisms. *Environ. Sci. Technol.* **2012**, *46*, 5912−5920.
(69) Sarpong, L. K.; Bredol, M.; Schönhoff, M. Heteroaggregation of Multiwalled Carbon Nanotubes and Zinc Sulfide Nanoparticles. *Carbon* **2017**, *125*, 480−491.
(70) Li, F.; Zhang, Q.; Klumpp, E.; Bol, R.; Nischwitz, V.; Ge, Z.; Liang, X. Organic Carbon Linkage with Soil Colloidal Phosphorus at Regional and Field Scales: Insights from Size Fractionation of Fine Particles. *Environ. Sci. Technol.* **2021**, *55*, 5815−5825.
(71) Missong, A.; Bol, R.; Nischwitz, V.; Krüger, J.; Klumpp, E. Phosphorus in Water Dispersible-Colloids of Forest Soil Profiles. *Plant Soil* **2017**, *2*, 71−86.
(72) Jiang, X.; Bol, R.; Nischwitz, V.; Siebers, N.; Willbold, S.; Vereecken, H.; Amelung, W.; Klumpp, E. Phosphorus Containing Water Dispersible Nanoparticles in Arable Soil. *J. Environ. Qual.* **2015**, *44*, 1772−1781.
(73) Monikh, F. A.; Grundschober, N.; Romeijn, S.; Arenas-Lago, D.; Vijver, M. G.; Jiskoot, W.; Peijnenburg, W. J. G. M. Development of Methods for Extraction and Analytical Characterization of Carbon-Based Nanomaterials (Nanoplastics and Carbon Nanotubes) in Biological and Environmental Matrices by Asymmetrical Flow Field-Flow Fractionation. *Environ. Pollut.* **2019**, *255*, No. 113304.
(74) Bradford, S. A.; Kim, H.; Shen, C.; Sasidharan, S.; Shang, J. Contributions of Nanoscale Roughness to Anomalous Colloid Retention and Stability Behavior. *Langmuir* **2017**, *33*, 10094−10105.
(75) Torkzaban, S.; Bradford, S. A. Critical Role of Surface Roughness on Colloid Retention and Release in Porous Media. *Water Res.* **2016**, *88*, 274−284.
(76) Gomez-Flores, A.; Bradford, S. A.; Wu, L.; Kim, H. Interaction Energies for Hollow and Solid Cylinders: Role of Aspect Ratio and Particle Orientation. *Colloids Surf., A* **2019**, *580*, No. 123781.

https://doi.org/10.1021/acs.est.2c00681
Environ. Sci. Technol. XXXX, XXX, XXX−XXX

(77) Shen, C.; Bradford, S. A.; Wang, Z.; Huang, Y.; Zhang, Y.; Li, B. DLVO Interaction Energies between Hollow Spherical Particles and Collector Surfaces. *Langmuir* **2017**, *33*, 10455−10467.
(78) Shen, C.; Bradford, S. A.; Flury, M.; Huang, Y.; Wang, Z.; Li, B. DLVO Interaction Energies for Hollow Particles: The Filling Matters. *Langmuir* **2018**, *34*, 12764−12775.
(79) Lefrant, S.; Baibarac, M.; Baltog, I. Raman and FTIR Spectroscopy as Valuable Tools for the Characterization of Polymer and Carbon Nanotube Based Composites. *J. Mater. Chem.* **2009**, *19*, 5690−5704.
(80) Selvin, T. P.; Girei, S. A.; Al-Juhani, A. A.; Mezghani, K.; De, S. K.; Atieh, M. A. Effect of Phenol Functionalized Carbon Nanotube on Mechanical, Dynamic Mechanical, and Thermal Properties of Isotactic Polypropylene Nanocomposites. *Polym. Eng. Sci.* **2012**, *52*, 525−531.
(81) Çalışır, Ü.; Çiçek, B. Synthesis of Thiol-Glycol-Functionalized Carbon Nanotubes and Characterization with FTIR, TEM, TGA, and NMR Technics. *Chem. Pap.* **2020**, *74*, 3293−3302.
(82) Villalobos, M.; Leckie, J. O. Surface Complexation Modeling and FTIR Study of Carbonate Adsorption to Goethite. *J. Colloid Interface Sci.* **2001**, *235*, 15−32.
(83) Fu, H.; Xie, Q. Complexes of Fulvic Acid on the Surface of Hematite, Goethite, and Akaganeite: Ftir Observation. *Chemosphere* **2006**, *63*, 403−410.
(84) Kang, S.; Xing, B. Humic Acid Fractionation Upon Sequential Adsorption onto Goethite. *Langmuir* **2008**, *24*, 2525−2531.
(85) Gupta, A.; Srivastava, C. Nucleation and Growth Mechanism of Tin Electrodeposition on Graphene Oxide: A Kinetic, Thermodynamic and Microscopic Study. *J. Electroanal. Chem.* **2020**, *861*, No. 113964.
(86) Gottschalk, F.; Sonderer, T.; Scholz, R. W.; Nowack, B. Modeled Environmental Concentrations of Engineered Nanomaterials (TiO_2, ZnO, Ag, CNT, Fullerenes) for Different Regions. *Environ. Sci. Technol.* **2009**, *43*, 9216−9222.
(87) Gottschalk, F.; Nowack, B. The Release of Engineered Nanomaterials to the Environment. *J. Environ. Monit.* **2011**, *13*, 1145−1155.
(88) Mansor, M. M.; Drabesch, S.; Bayer, T.; Le, A. V.; Chauhan, A.; Schmidtmann, J.; Peiffer, S.; Kappler, A. Application of Single-Particle ICP-MS to Determine the Mass Distribution and Number Concentrations of Environmental Nanoparticles and Colloids. *Environ. Sci. Technol. Lett.* **2021**, *8*, 589−595.
(89) Zhao, W.; Zhao, P.; Tian, Y.; Shen, C.; Li, Z.; Peng, P.; Jin, C. Investigation for Synergies of Ionic Strength and Flow Velocity on Colloidal-Sized Microplastic Transport and Deposition in Porous Media Using the Colloidal−AFM Probe. *Langmuir* **2020**, *36*, 6292−6303.
(90) Zhu, S.; Huang, X.; Yang, X.; Peng, P.; Li, Z.; Jin, C. Enhanced Transformation of Cr(Vi) by Heterocyclic-N within Nitrogen-Doped Biochar: Impact of Surface Modulatory Persistent Free Radicals (PFRs). *Environ. Sci. Technol.* **2020**, *54*, 8123−8132.

https://doi.org/10.1021/acs.est.2c00681
Environ. Sci. Technol. XXXX, XXX, XXX−XXX